J Solid State Electrochem (2012) 16:3087–3096
DOI 10.1007/s10008-012-1750-3

ORIGINAL PAPER

Smart synthesis of hollow core mesoporous shell carbons (HCMSC) as effective catalyst supports for methanol oxidation and oxygen reduction reactions

J. Zeng · C. Francia · C. Gerbaldi · M. A. Dumitrescu · S. Specchia · P. Spinelli

Received: 5 December 2011 / Revised: 6 April 2012 / Accepted: 9 April 2012 / Published online: 26 April 2012

Abstract The present paper describes an easy and quick synthesis of hollow core mesoporous shell carbon (HCMSC) simply templated from unpretreated solid core mesoporous shell silica using a cheap precursor like sucrose. Physical characterizations showed uniform spherical carbon capsules with a hollow macroporous core of ca. 305- and 55-nm-thick mesoporous shell, forming a well-developed 3-D interconnected bimodal porosity. High specific surface area and large pore volume were also confirmed, suggesting the obtained HCMSC as a promising catalyst support. HCMSC-supported Pt (nominal 20 wt.%) with an average Pt particle size of 1.9 nm was synthesized by wet impregnation, and a signal of strong interaction between carbon support and platinum was confirmed by X-ray photoelectron spectroscopy. In cyclic voltammetry and linear sweep voltammetry tests, the Pt/HCMSC electrode showed significantly higher electrocatalytic activity for methanol oxidation reaction (MOR) and oxygen reduction reaction (ORR) if compared with commercial Pt/Vulcan catalyst. The durability tests by cyclic voltammetry showed for the Pt/HCMSC a lower electrochemical active surface area loss than the commercial one in acidic solution. All the primary tests suggested that the Pt/HCMSC, due to its particular structure and the high dispersion of noble metal particles, is a promising catalyst for fuel cell applications, for MOR and ORR.

J. Zeng · C. Francia · C. Gerbaldi · M. A. Dumitrescu · S. Specchia (✉) · P. Spinelli
Department of Applied Science and Technology,
Politecnico di Torino,
Corso Duca degli Abruzzi 24,
10129, Turin, Italy
e-mail: stefania.specchia@polito.it

Keywords Hollow core mesoporous shell carbon (HCMSC) · Platinum · Methanol oxidation reaction (MOR) · Oxygen reduction reaction (ORR) · Durability · Fuel Cell electrocatalyst

Introduction

Since the introduction of fuel cells (FCs) technology, carbon materials have been widely studied as supports for precious metals catalysts (e.g., Pt, Pd, Ru, etc.) [1–4]. As suitable supports for FC catalysts, carbon materials should possess high specific surface area, good electrical conductivity, diffusion-favored porosity, and high stability in FCs environment. Up to 1990s, the most commonly used catalyst support in low-temperature FCs was carbon black (e.g., Vulcan XC-72R, Black Pearls, and Denka Black [3]). However, in order to improve the electrochemical activity and stability of the supported catalysts, new carbon materials with controlled and tunable nanostructures have been abundantly developed, as summarized in the literature [5]. Ordered mesoporous carbons (OMCs) with narrow pore-size distributions (PSDs), high specific surface areas (up to 1,800 $m^2\ g^{-1}$), and large pore volumes were successfully templated from silicas and used as novel catalyst supports in FCs [4, 6–8]. Generally, metal-supported OMCs presented high metal dispersion because of the high specific surface area, good mass transfer because of the ordered porosity, but low metal accessibility because of the presence of Pt located into the pores without Nafion® ionomer access [9]. Carbon nanotubes have been deeply investigated as catalyst supports for low-temperature FCs because of their high electronic conductivity, large specific surface area, and high stability [10]. However, the high cost and the complexity of the synthesis methods hindered the commercialization of

carbon nanotubes. Carbon nanohorns, carbon nanocoils, and carbon fibers have also been studied as FC catalyst supports and showed promising results [11–13].

Hierarchically porous carbons, especially those possessing well-defined macropores and interconnected meso- and/or micropores, attracted much attention because of their excellent performance of mass transport from macropores and their high specific surface areas from micro-/mesopores [14–17]. Ren et al. [15] reported a dual-porosity carbon with a high specific surface area (>1,000 $m^2\ g^{-1}$) as well as large pore volume (>1.2 $cm^3\ g^{-1}$), and its corresponding PtRu/C catalyst demonstrated a higher activity toward methanol oxidation reaction (MOR) than commercial electrocatalysts. Chen et al. [16] also demonstrated that bimodal porous carbon materials with three dimensionally interconnected structures were promising supports in FC application. In the last decade, since firstly reported by Yoon et al. in 2002 [17], a unique dual-porosity carbon structure with macroporous hollow cores and mesoporous shells, named hollow core mesoporous shell carbon (HCMSC), was considered to be promising for FC application as catalyst support [18–21]. In their synthesis, HCMSCs were templated from pre-treated solid core mesoporous shell (SCMS) silica with phenol-paraformaldehyde resin or divinylbenzene/azo-bis-isobutyronitrile (DVB/AIBN) as precursors. However, the incorporation of the reactive species (e.g., aluminum oxide) onto the mesoporous silica template and use of complicated precursors (e.g., DVB/AIBN) resulted in a tedious process and high costs for carbon production.

In the present work, a novel and smart method to synthesize HCMSC with high specific surface area and large pore volume is proposed, using unpretreated SCMS silica as template and cheap sucrose as the carbon precursor. To the best of our knowledge, such a quick and inexpensive method has not been reported so far. The obtained carbon material was used as the support for platinum loading. The dispersion of platinum nanoparticles, the MOR, the oxygen reduction reaction (ORR), and the durability of the supported catalyst were systematically investigated and compared with those of commercial Pt/Vulcan.

Experimental

Synthesis of SCMS silica and HCMSC

Mesoporous materials were intensively developed using different organic and block copolymer surfactants [22, 23]. In this work, submicrometer-sized solid core mesoporous shell (SCMS) silica was synthesized from the simultaneous polymerization of tetraethoxysilane (TEOS) and octadecyltrimethoxysilane (C_{18}TMS) followed by removal of the organic group, according to the procedure reported by Buchel et al. [24]. Firstly, 6.3 ml of aqueous ammonia (32 wt.%, Sigma Aldrich) was added into a solution containing 150 ml of ethanol and 20 ml of doubly distilled water. After stirring for 15 min, 12 ml of TEOS (98 wt.%, Sigma Aldrich) was added at 30 °C under vigorous stirring, and the above mixture was stirred for 6 h to yield uniform silica spheres. Then, a mixture containing 10 ml of TEOS and 4 ml C_{18}TMS (90 wt.%, Sigma Aldrich) was added into the colloidal solution containing silica spheres and further reacted for 1 h. The final SCMS silica material was retrieved by centrifugation and further calcined at 550 °C for 6 h under oxygen atmosphere.

HCMSCs were synthesized using a hard templating method: 1 g of SCMS silica was added to a solution containing 0.63 g of sucrose, 0.07 g of H_2SO_4 (97–98 wt.%, Sigma Aldrich), and 2.5 g of H_2O. The mixture was kept in an oven for 6 h at 100 °C, and subsequently, the temperature was increased to 160 °C and maintained for another 6 h. The heating procedure was repeated after the addition of 0.4 g of sucrose, 0.05 g of H_2SO_4, and 2.5 g of H_2O, in order to completely infiltrate the internal pores of SCMS silica with carbon. The carbon–silica composite was obtained after pyrolysis at 900 °C for 6 h and then washed in 5 wt.% HF (Sigma Aldrich) solution to remove silica template.

Preparation of Pt/HCMSC catalyst

Dispersion of the catalytic metal on the HCMSC was achieved by wet impregnation technique. A solution of chloroplatinic acid hexahydrated ($H_2PtCl_6{\cdot}6H_2O$, Sigma Aldrich) in acetone was added dropwise to the carbon powder. The mixture was ultrasonicated for 30 min and then stirred for 2 h. The slurry was then heated at 60 °C, with continuous stirring, in order to evaporate the excess acetone. The amount of acid in the solution depended on the desired platinum content in the catalyst [25]. The sample was then treated under H_2 flow at 300 °C for 2 h in order to reduce the $PtCl_6^{2-}$ ions to metallic Pt. In this work, HCMSC-supported catalysts were prepared and denoted as Pt/HCMSC, with a nominal 20 wt.% of Pt loading. A commercial 20 wt.% Pt/Vulcan electrocatalyst (E-Tek) was used for comparison tests. The nominal and commercial values included all the Pt content without distinguishing between oxidized or metal Pt.

Surface characterization

The morphology of the samples was examined using a FEI inspect S50/EDAX. Field emission scanning electron microscope (FESEM; model JEOL JSM 6700F) was also employed to determine the surface morphology and spheres sizes. Nitrogen adsorption isotherms at 77 K were recorded by an ASAP2010 Instrument (Micromeritics). The specific surface area (SSA) of the samples was calculated through

the Brunauer–Emmet–Teller (BET) method within the relative pressure range of 0.05 to 0.2 [26]. The PSD was obtained with the Barrett–Joyner–Halenda (BJH) method calibrated for cylindrical pores according to the improved Kruk–Jaroniec–Sayari (KJS) method [27].

The X-ray diffraction (XRD) patterns were collected with a Philips X-Pert MPD X-ray diffractometer equipped with a Cu Kα radiation and 0.02° step size (6 s step time) at 40 kV and 30 mA. High-resolution transmission electron microscopy (HRTEM; model JEOL JEM 2010) was employed for estimation of the platinum particle size and distribution in the carbon supported catalysts. X-ray photoelectron spectroscopy (XPS) measurements were carried out using a Physical Electronics PHI 5800 (USA) multi-technique ESCA system (with monochromatic Al-Kα X-ray radiation). The survey and narrow spectra were obtained with energy of 187.8 and 23.5 eV, respectively. The samples were placed in an ultrahigh vacuum chamber at 2×10^{-10} Torr.

The platinum-to-carbon weight percentage in the catalysts was determined by inductively coupled plasma atomic emission spectroscopy (ICP-AES) with a Varian Liberty 100 instrument. Prior to analysis, the samples were digested in hot concentrated HCl/HNO_3=3:1 mixture.

Electrochemical characterization and accelerated degradation tests

Electrochemical measurements were carried out on an electrochemical workstation (CHI 600D series) at room temperature in a three-electrode system. An Ag/AgCl (1.0 M Cl^-) electrode and a Pt wire were used as reference electrode and counter electrode, respectively. The calculation of the Ag/AgCl reference electrode potential in 1.0 M KCl solution compared to the reversible hydrogen electrode (RHE) provided the value of 0.255 V. Cyclic voltammetries (CVs) were conducted in N_2-saturated 0.5 M H_2SO_4 solution with or without 1.0 M CH_3OH at a scan rate of 10 mV s^{-1}. Chronoamperometric experiments were carried out in 0.5 M H_2SO_4 solution with 1 M CH_3OH at room temperature, with the electrode potential fixed at 0.6 V (vs. Ag/AgCl). A glassy carbon covered with a thin layer of Nafion®-impregnated catalyst (geometrical area 0.076 cm^2) was employed as the working electrode. Prior to measurement, N_2 was bubbled directly into the cell for at least 15 min to saturate the solution. Potential cycling is a common accelerated degradation test for electrocatalysts of FC because it is simple and time-effective [28–31]. The working electrode was cycled between 0.2 and 1.0 V (vs. Ag/AgCl) at a scan rate of 1.0 V s^{-1} in N_2-saturated 0.5 M H_2SO_4 solution. The potential range of 0.2–1.0 V (vs. Ag/AgCl) for accelerated degradation tests assured the accelerated corrosion of carbon supports as well as the sintering of Pt nanoparticles based on the protocol suggested by DOE [32] and other literature papers [28, 33]. The cyclic voltammograms were recorded at a scan rate of 10 mV s^{-1} after every 1,000 consecutive potential cycles. The hydrogen desorption peak area was used to quantify the electrochemical active surface area (EASA). Linear sweep voltammetry (LSV) was performed in O_2-saturated 0.5 M H_2SO_4 solution at a scan rate of 5 mV s^{-1}. A rotating glassy carbon disk covered with a thin layer of Nafion®-impregnated catalyst (geometrical area 0.126 cm^2) was used as the working electrode, and the rotation rate of the disk varied between 100 and 2,500 rpm. Oxygen was bubbled directly into the cell for at least 30 min before the test and was flushed over the cell solution during the measurement.

Both the working electrodes for CVs and LSVs were prepared with the same procedure as follows: 5.0 mg of catalyst (Pt/Vulcan or Pt/HCMSC) was mixed with 0.1 ml of ethanol, 0.1 ml of isopropanol, and 30 μl of Nafion® solution (5 wt.%, Quintech). The mixture was sonicated for 30 min to obtain the ink slurry. Then 5 μl of the slurry was applied to the surface of each the glassy carbon electrodes (0.076 and 0.126 cm^2, respectively), and the lined electrodes were kept at room temperature for 1 h before use. The obtained results from the analyses were then normalized per milligram of Pt.

Results and discussion

Surface characterization of HCMSC and Pt/HCMSC catalysts

The morphological characterization of SCMS silica and HCMSC supports was performed by SEM and FESEM. Figure 1 shows representative SEM images of the SCMS silica and HCMSC. In Fig. 1a, most of the SCMS silica particles were spherical and uniform with an average particle size of 430 nm, while the HCMSC (Fig. 1b) showed a smaller particle size of ca. 410 nm, indicating a slight shrinkage compared to its parent silica template. The FESEM images (Fig. 1c, d) confirm that the HCMSC had a hollow core diameter of ca. 305 nm and shell thickness of ca. 55 nm.

Nitrogen adsorption–desorption isotherms for SCMS and HCMSC are shown in Fig. 2a, which can be classified as a type IV isotherm with H_2-type hysteresis according to the International Union of Pure and Applied Chemistry nomenclature. Surface structural parameters for the HCMSC and Vulcan are summarized in Table 1. The SCMS silica possessed a rather small SSA of 326 $m^2\ g^{-1}$ as well as a quite low pore volume (Fig. 2b), whereas the corresponding HCMSC exhibited a large SSA of 1,258 $m^2\ g^{-1}$ and a total pore volume of 1.06 $cm^3\ g^{-1}$ (Table 1), which were mainly attributed to the presence of the mesopores in the shell. A narrow PSD centered at ca. 3.3 nm was estimated for the mesopores in the HCMSC. From Table 1, it is evident that the porosity of HCMSC prepared from sucrose was similar to that prepared

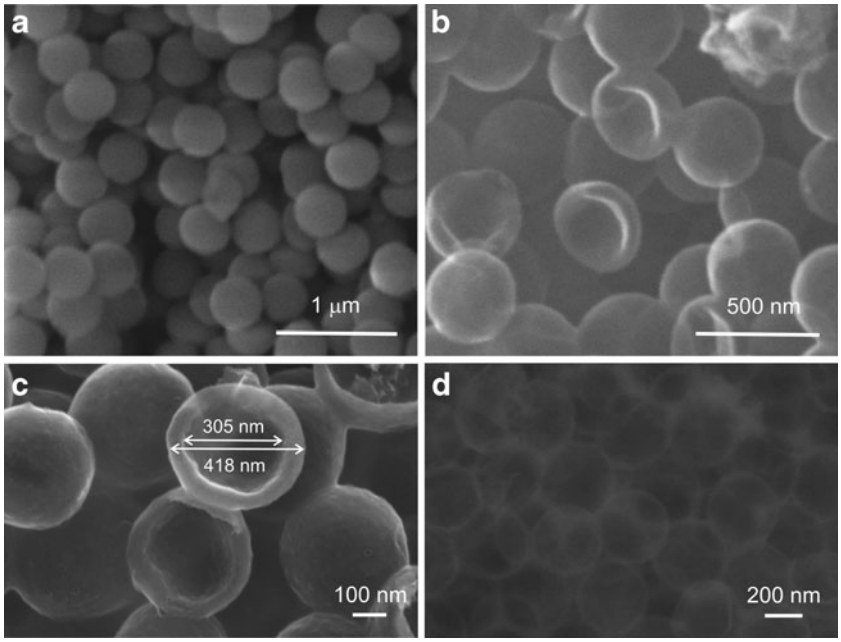

Fig. 1 SEM micrographs of SCMS silica (**a**) and its carbon replica HCMSC (**b**); FESEM micrographs of HCMSC (**c**, **d**)

from phenol-paraformaldehyde resin (HCMSC 1 [20]) but possessed a much higher SSA than the one synthesized from divinylbenzene/azobis-isobutyronitrile (HCMSC 2 [21]). All the HCMSCs exhibited much larger SSA and mesopore volume than the Vulcan (E-Tek [18]). Additionally, each carbon capsule of the HCMSC had a bimodal pore system composed of a spherical macroporous core and mesopores in the shell connecting inside and outside of the hollow core, while Vulcan exhibited an appreciable amount of micropores (<2 nm) except for the randomly distributed mesopores and macropores with varying sizes.

XRD patterns for Pt/HCMSC and commercial Pt/Vulcan electrocatalysts are shown in Fig. 3. Both XRD patterns of the Pt/C electrocatalysts exhibited the main characteristic peaks of FCC crystalline Pt with planes of (111), (200), (220), and (311) located at 39.5°, 46.3°, 67.5°, and 81.5° in the 2θ axis [34]. The first broad peak at 2θ of 23.9° belonged to the carbon support.

From HRTEM images of Pt/HCMSC, at both low (Fig. 4a) and high magnification (Fig. 4b), the platinum particles appeared well homogeneously and highly dispersed on the HCMSC surface: Both the external shell and the internal core of the support resulted completely covered by nanosized metal particles. The evaluation of the platinum particle distribution was performed on the higher-magnification HRTEM picture (Fig. 4b), as shown in Fig. 5: The particle size distribution appeared very narrow, centered on a mean particle size of 1.9 nm, with very low standard deviation. Moreover, the Pt particles incorporated on HCMSC were found to be smaller than those in the commercial Pt/Vulcan catalyst (2.4 nm [35]), due to the much higher SSA of the HCMSC. Determined by ICP-AES analysis, the overall Pt percentage in the synthesized Pt/HCMSC was 16.7 wt.%, whereas the Pt percentage of the commercial Pt/Vulcan was 19.6 wt.%.

The Pt oxidation state and the interaction between carbon support and platinum metal were determined by XPS. The XPS referred to a *C* 1s value of 284.6 eV. As shown in Fig. 6a, the Pt 4f peaks were deconvoluted into Pt $4f_{7/2}$ and Pt $4f_{5/2}$ doublets labeled as 1, 2, 3 and 1′, 2′, 3′, with the corresponding binding energy and relative ratio listed in Table 2. The most intensive doublet, namely 1 and 1′, was attributed to metallic platinum [36]. The second intensive

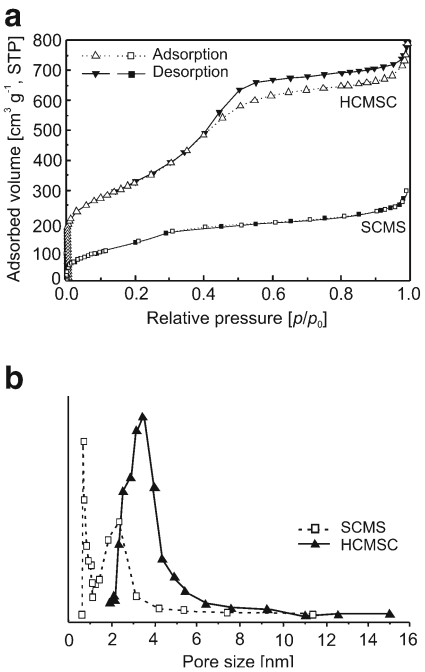

Fig. 2 N_2 adsorption/desorption isotherms (**a**) and particle size distribution (**b**) of HCMSC and SCMS

Table 1 Surface characterization of Pt/HCMSC and Pt/Vulcan from BET and BJH analyses

Carbon support	SSA ($m^2\ g^{-1}$)	D_{BJH} (nm)	V_{total} ($cm^3\ g^{-1}$)	V_{micro} ($cm^3\ g^{-1}$)
HCMSC	1258	3.3	1.06	0.21
Vulcan [18]	230	–	0.31	0.09
HCMSC1 [20]	1290	3.0	0.80	–
HCMSC2 [21]	759	3.9	0.99	–

doublet, namely 2 and 2′, belonged to PtO or $Pt(OH)_2$, as reported by Kim et al. [37]. The last doublet showed quite low intensity, which was assigned to $PtO_2{\cdot}xH_2O$ or $Pt(OH)_4$ [38]. The fraction of metallic platinum on the surface, Pt(0)s, can be evaluated from the intensity of the first doublet (1 and 1′). It can be seen that Pt/HCMSC catalyst displayed a higher Pt(0)s value than the commercial Pt/Vulcan catalyst, indicating more active sites and a higher catalytic activity for the former [39]. Furthermore, the binding energies of Pt 4f peak for Pt/HCMSC catalyst increased by 0.2 eV when compared to that for Pt/Vulcan, as shown in Fig. 6b. The observed slight shift of the doublet to higher binding energies might be a signal of stronger carbon support/platinum interaction [20, 28]. For Pt/HCMSC catalyst, the smaller Pt particles were likely to have higher fraction of surface atoms interacting with the carbon support, compared to larger particles, and thus stronger interaction was induced between metal particles and carbon support.

Electrochemical characterization on the activity of Pt/HCMSC catalyst

The cyclic voltammograms of Pt/HCMSC and Pt/Vulcan are shown in Fig. 7, together with their respective carbon supports only. The double layer capacitance of Pt/HCMSC catalyst increased due to the higher SSA of the HCMSC support. The EASA of Pt nanoparticles can be obtained from the hydrogen electrooxidation peaks after subtraction

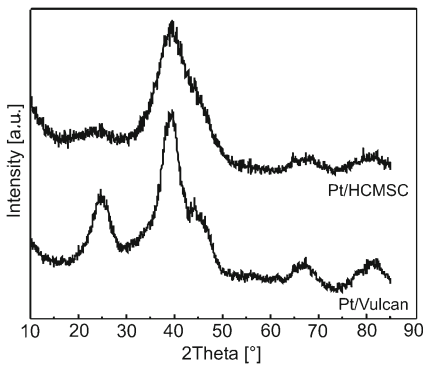

Fig. 3 XRD spectra of Pt/HCMSC and Pt/Vulcan catalysts

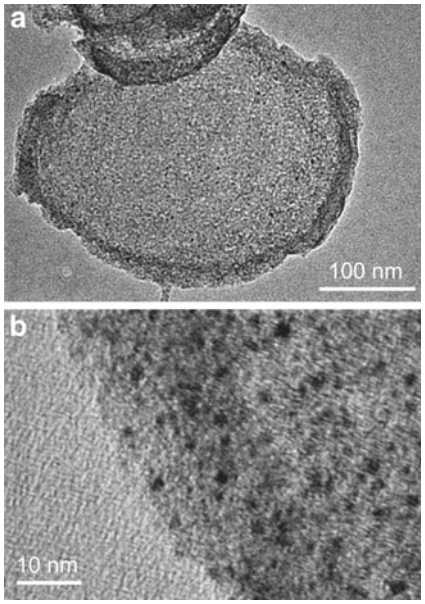

Fig. 4 HRTEM micrographs of Pt/HCMSC at low (**a**) and high (**b**) magnifications

of the double layer capacitance, by using the following equation (Eq. 1) [40, 41]:

$$\mathrm{EASA} = \frac{Q_H}{0.21 \cdot [\mathrm{Pt}]} \tag{1}$$

where Q_H is the amount of charge during hydrogen desorption on the surface of Pt electrode (milli-Coulombs per square centimeter), as shown in Fig. 7a, b; [Pt] represents the platinum loading (grams per square meter) on the working electrode and 0.21 represents the Pt poly-crystallite hydrogen adsorption constant (milli-Coulombs per square centimeter). The obtained EASA were 120.1 $m^2\ g_{Pt}^{-1}$ for Pt/HCMSC and 66.0 $m^2\ g_{Pt}^{-1}$ for Pt/Vulcan, respectively, as listed in Table 3. The theoretical specific surface area (TSSA) for Pt particles was also calculated from the crystallite size determined from the HRTEM particle size distribution, using the following equation (Eq. 2) [42]:

$$\mathrm{TSSA} = \frac{6}{\rho \cdot d} \tag{2}$$

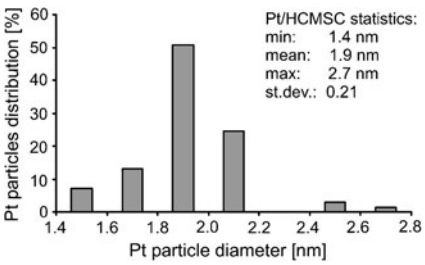

Fig. 5 Platinum particle size distribution of Pt/HCMSC evaluated from Fig. 4b

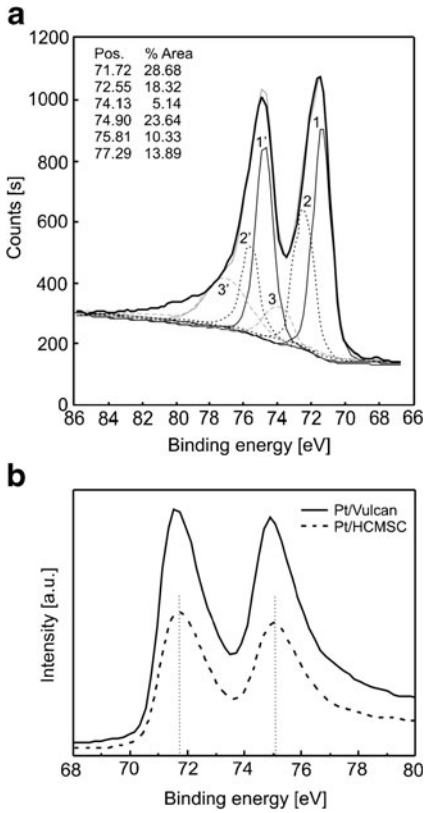

Fig. 6 Deconvolution of XPS Pt 4f spectra for Pt/HCMSC (**a**); comparison of Pt 4f spectra for Pt/HCMSC and Pt/Vulcan catalysts (**b**)

where ρ is the density of platinum (21.4×10^6 g m^{-3}) and d is the mean diameter of the particle (meters) determined from HRTEM for Pt/HCMSC catalyst and taken from literature [35] for Pt/Vulcan catalyst (see Table 2). The Pt utilization efficiency, E_{Pt}, of the catalysts calculated from EASA and TSSA is also reported in Table 3. The EASA calculated from CVs exhibited some losses compared with the TSSA from the HRTEM, which was probably attributed to the blocking or anchoring of the Nafion® on the surface of Pt particles and to the inaccessibility of catalyst deep inside the micropores of the carbon support [43]. It should be noted that E_{Pt} for Pt/HCMSC catalysts was 24.9 % higher than that of Pt/Vulcan catalyst. The high E_{Pt} of Pt/HCMSC resulted partly from the uniform dispersion of Pt nanoparticles with small size (average 1.9 nm) and partly from the narrow-size distribution of mesopores (between 2.0 and 4.0 nm) on HCMSC support. Additionally, the unique well-combined bimodal nanoporous structure of HCMSC, providing more efficient mass transport networks around Pt nanoparticles, could also contribute to the higher Pt utilization efficiency of Pt/HCMSC electrocatalyst.

The electrochemical catalytic activities of Pt/HCMSC and commercial Pt/Vulcan toward MOR were investigated through CV. Prior to analysis, the electrodes were placed in the N_2-saturated 0.5 M H_2SO_4 and 1.0 M CH_3OH aqueous solution for about 10 min to allow the system reaching a stable state. The CV curves of Pt/HCMSC for MOR were obtained after about 10 cycles and compared with Pt/Vulcan under the same condition as shown in Fig. 8. For both catalysts, the peaks observed at about 0.69–0.77 V in the forward scan (I_f) were characteristic of MOR [44], whereas the peaks at about 0.45–0.46 V in the reverse scan (I_b) were primarily associated with removal of the residual carbon species formed in the forward scan [45]. The I_f/I_b value, which was usually applied as an index to evaluate the tolerance of catalyst to CO poisoning [46] was calculated and listed in Table 3. A higher I_f/I_b value suggested that a higher amount of methanol was completely oxidized to carbon dioxide [47]. The catalyst Pt/HCMSC exhibited an I_f/I_b of 1.95, which was much higher than that of Pt/Vulcan (I_f/I_b=0.87), indicating higher efficiency toward MOR for the former. The potential of the methanol oxidation peak (I_f) can also be used to evaluate the catalysts' activity. The lower peak potential is usually thought to result from higher MOR activity of the catalyst [48, 49]. However, this potential is not always considered especially when catalyst supports with high BET SSA are involved. The supported catalysts with higher activity could have positively shifted MOR peak [18, 50–52]. In addition, this peak potential is also dependent on the Pt loading of the GC electrode, which is not the intrinsic property of the catalyst [53]. On the contrary, the magnitude of the peak current density (I_f) is directly proportional to the amount of methanol oxidized at the electrode and is commonly used to evaluate the activity of the catalyst toward MOR [50, 53, 54].

The Pt/HCMSC presented a maximum mass activity (MA_{max}) of 275.8 mA mg_{Pt}^{-1} toward MOR, which was significantly higher than that for Pt/Vulcan (169.6 mA mg_{Pt}^{-1}).

Table 2 Characterization of Pt/HCMSC and Pt/Vulcan from HRTEM and XPS analyses

Electrocatalyst	Mean Pt particle size (nm)	Pt $4f_{7/2}$		Pt $4f_{5/2}$		Percentage of metallic Pt on the surface (Pt(0)s %)
		Binding energy (eV)	Relative ratio (%)	Binding energy (eV)	Relative ratio (%)	
Pt/HCMSC	1.9	71.52	28.68	74.90	23.64	52.32
Pt/Vulcan	2.4[a]	71.50	29.45	74.82	19.74	49.19

[a] Value taken from [35]

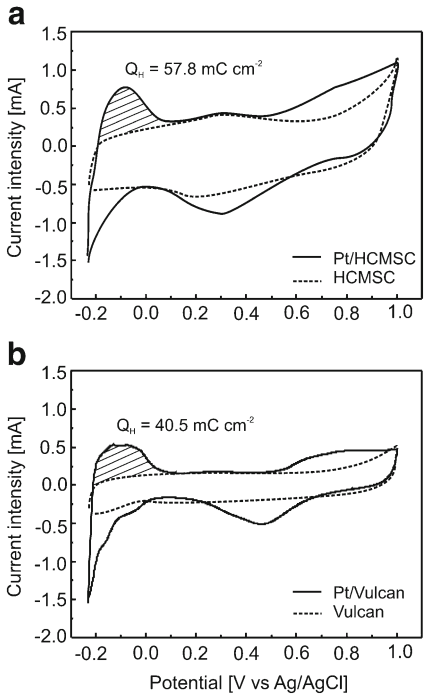

Fig. 7 Cyclic voltammograms of Pt/HCMSC and Pt/Vulcan

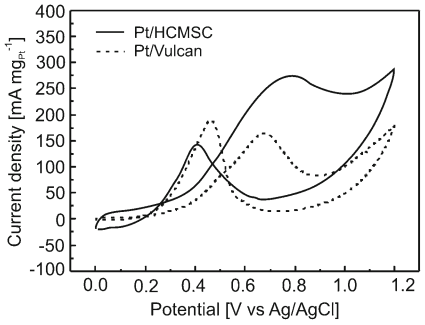

Fig. 8 Methanol oxidation reaction for Pt/HCMSC and Pt/Vulcan

The increased value in mass-normalized current density indicated that the Pt catalyst supported on HCMSC had an enhanced intrinsic activity toward MOR.

Figure 9 shows the chronoamperometric curves of the two catalysts toward MOR at 0.6 V. Both catalysts showed a decay in the methanol oxidation current with time, which may result from the poison of intermediate species on Pt active sites [55]. Pt/HCMSC catalyst showed a little slower decay rate and higher activity than the Pt/Vulcan catalyst during the 50-min testing, evidencing that the Pt/HCMSC catalyst exhibited an enhanced catalytic activity toward methanol oxidation.

The superior catalytic activity of Pt/HCMSC toward MOR could be due to the higher Pt utilization efficiency determined by CV and the unique pore structure minimizing mass diffusion limitations [56]. This HCMSC material synthesized from sucrose could be a promising catalyst support for effective electrocatalysts in direct methanol fuel cells (DMFCs) according to these primary results.

Figure 10 displays the LSV and Koutecky–Levich plots (at 0.6 and 0.65 V, respectively) of Pt/HCMSC and Pt/Vulcan catalysts at various rotating speeds of rotating disk electrode. As presented in the LSVs, the limiting currents of ORR on Pt/HCMSC were much higher than those on the Pt/Vulcan at the same scanning rates. The increase in the limiting current is associated with the increase of molecular oxygen diffusion through the electrode surface [57]. Therefore, the enhancement of ORR on Pt/HCMSC could be partly attributed to the diffusion-favored porosity of HCMSC support. The kinetic currents (I_{kin}) of Pt/HCMSC and Pt/Vulcan catalysts were calculated from Koutecky–Levich analysis at 0.65 and 0.6 V, respectively, and the mass activities were also derived from I_{kin}, as listed in Table 3. The mass activities of Pt/C catalysts were 0.025–0.031 A mg_{Pt}^{-1} at 0.60 V, which were similar to the activities of Pt/C (16.6 wt.%) and Pt/OMC (11.5 wt.%) catalysts reported by Elezovic et al. [58], and Zeng et al. [8], respectively, and also in the range of 0.020–0.045 A mg_{Pt}^{-1} for Pt/OMCs (60.0 wt.%) reported by Joo et al. [59]. The kinetic currents and mass activities of Pt/HCMSC were higher than those of Pt/Vulcan, indicating the higher catalytic activity toward

Table 3 Electrochemical characterization of Pt/HCMSC and Pt/Vulcan from CV, MOR, and ORR analyses

Electrocatalyst	EASA (m^2 g^{-1})	TSSA (m^2 g^{-1})	E_{Pt} (%)	MOR		ORR			
				I_f/I_b (–)	MA_{max} (mA mg_{Pt}^{-1})	0.6 V		0.65 V	
						I_{kin} (mA)	MA (A mg_{Pt}^{-1})	I_{kin} (mA)	MA (A mg_{Pt}^{-1})
Pt/HCMSC	120.1	147.6	81.4	1.95	275.8	0.57	0.031	0.242	0.013
Pt/Vulcan	66.0	116.8	56.5	0.87	169.6	0.53	0.025	0.192	0.0089

EASA electrochemical active surface area of Pt particles, *TSSA* theoretical specific surface area of Pt particles, E_{Pt} Pt utilization efficiency of the catalysts calculated as EASA/TSSA, I_f/I_b ratio between the peak observed in the forward scan (I_f) and peak observed in the backward scan (I_b), MA_{max} maximum mass activity toward methanol oxidation reaction derived from maximum current density, I_{kin} kinetic current intensity for oxygen reduction reaction calculated from Koutecky–Levich, *MA* mass activity toward oxygen reduction reaction derived from I_{kin}

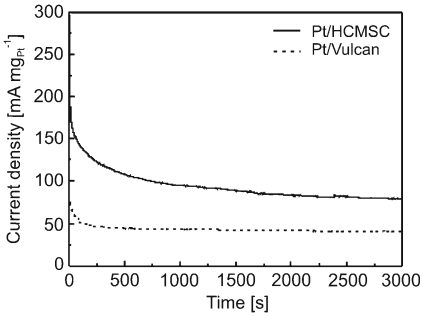

Fig. 9 Chronoamperometric curves of Pt/HCMSC and Pt/Vulcan for methanol electrooxidation in 0.5 M H_2SO_4 solution with 1 M CH_3OH at room temperature at 0.6 V (vs. Ag/AgCl)

ORR for the former. The metal/support interaction may be partly responsible for the change of the mass activity. The stronger interaction for Pt/HCMSC could enhance charge transfer between carbon support and Pt particles, eventually positively affected the catalytic activity.

Accelerated degradation tests on the durability of Pt/HCMSC catalyst

The electrocatalysts stability is one of the most important issues in the development of supported catalysts for FC application [60]. Carbon corrosion is considered to be a vital cause of cathode degradation in proton exchange membrane fuel cells (PEMFCs), which usually operates in a potential window of 0.6–1.0 V (vs. SHE). The anode of DMFC, operating around 0.4 V (vs. SHE), is also susceptive to carbon support corrosion [61]. Another issue related to the durability of FC catalysts is the sintering of Pt nanoparticles, by either a coalescence mechanism (aggregation of adjacent small particles by thermal motion during the electrochemical process) or an Ostwald ripening mechanism (dissolution of small Pt particles and recrystallization into a large parti-

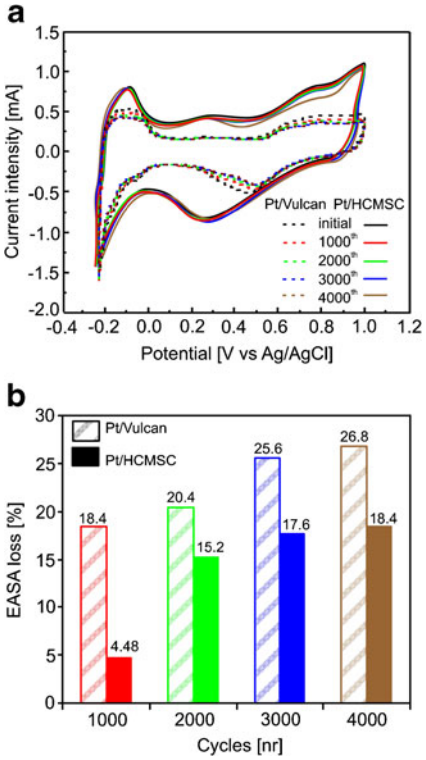

Fig. 11 Cyclic voltammograms for Pt/HCMSC and Pt/Vulcan after consecutive cycling (**a**) and the related loss of EASA (**b**)

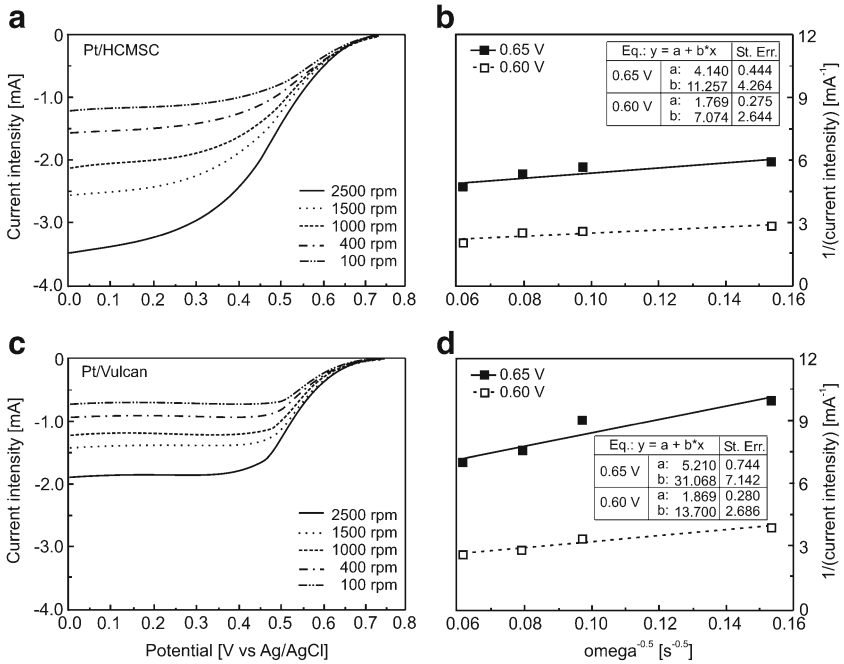

Fig. 10 Oxygen reduction reaction at various rpm (**a**, **c**) and Koutecky–Levich plots at 0.65 and 0.60 V (**b**, **d**) for Pt/HCMSC (**a**, **b**) and Pt/Vulcan (**c**, **d**)

cle) [3, 62–65]. To evaluate the stability of the supported catalysts, accelerated durability test was conducted by potential cycling. Figure 11a shows the CVs for Pt/HCMSC and Pt/Vulcan before cycling and after every 1,000 consecutive cycling. With cycling, a reduction on the hydrogen desorption–adsorption peaks was observed for both catalysts, indicating losses of EASA and catalyst degradations. After 4,000 potential cycles, the loss of EASA for Pt/Vulcan catalyst was 26.8 %, which was almost the 45.6 % more of that for Pt/HCMSC catalyst (18.4 %), as shown in Fig. 11b. The lower EASA loss for Pt/HCMSC was likely due to the stronger interaction between Pt and HCMSC support confirmed by XPS, which minimized the coalescence and Ostwald ripening of small Pt nanoparticles [63, 64]. The unique pore structure and high BET SSA of HCMSC support could be helpful to confine the sintering of Pt nanoparticles and improve the stability of the catalyst.

Conclusions

In the present work, HCMSC with a bimodal pore system composed of a hollow core and mesoporous shell was facilely synthesized by a liquid impregnation method, using cheap sucrose as carbon precursor and unpretreated SCMS silica as hard template. The prepared carbon materials with uniform spherical grains showed a narrow pore-size distribution, a high specific surface area, as well as a large pore volume in the framework. The HCMSC-supported catalyst (Pt/HCMSC) was prepared by solution impregnation with $H_2PtCl_6{\cdot}6H_2O$ and subsequent H_2 reduction. Smaller Pt particles, higher fraction of metallic state Pt, as well as stronger interaction between carbon and metal particles were detected for the Pt/HCMSC, compared with the commercial Pt/Vulcan catalyst. CV tests confirmed a high EASA and high Pt utilization efficiency for the Pt/HCMSC, due to the small uniformly dispersed Pt particles as well as the unique bimodal pore structure of the HCMSC support. The Pt/HCMSC was found to be more catalytic active toward methanol oxidation reaction and oxygen reduction reaction compared to the commercial catalyst Pt/Vulcan, which was consistent with its higher EASA and higher Pt utilization efficiency. From the accelerated degradation tests, the Pt/HCMSC showed less EASA loss than the commercial Pt/Vulcan. From the present results, HCMSC materials confirmed to be potential supports for FC electrocatalysts suitable for both PEMFCs (ORR reaction) and DMFCs (MOR reaction).

Acknowledgments Mr M. Raimondo (Politecnico di Torino), Dr E. Celasco (Politecnico di Torino), and Dr V. Baglio (CNR-ITAE, Messina, Italy) are gratefully acknowledged for SEM/XPS/HRTEM analysis.

References

1. Ramesh KV, Shukla AK (1987) J Power Sources 19:279–285
2. Honji A, Mori T, Hishinuma Y (1990) J Electrochem Soc 137:2084–2088
3. Uchida M, Aoyama Y, Tanabe M, Yanagihara N, Eda N, Ohta A (1995) J Electrochem Soc 142:2572–2576
4. Chang H, Joo SH, Pak C (2007) J Mater Chem 17:3078–3088
5. Antolini E (2009) Appl Catal B Environ 88:1–24
6. Wen Z, Liu J, Li J (2008) J Adv Mater 20:743–747
7. Wu H, Wexler D, Wang G, Liu H (2012) J Solid State Electrochem 16:1105–1110
8. Zeng J, Francia C, Dumitrescu MA, Monteverde Videla AHA, Ijeri VS, Specchia S, Spinelli P (2011) Electrochemical performance of Pt-based catalysts supported on different ordered mesoporous carbons (Pt/OMCs) for oxygen reduction reaction. Ind Chem Eng Res. doi:10.1021/ie2016619
9. Ding J, Chan KY, Ren JW, Xiao FS (2005) Electrochim Acta 50:3131–3141
10. Wei ZD, Yan C, Tan Y, Li L, Sun CX, Shao ZG, Shen PK, Dong HW (2008) J Phys Chem C 112:2671–2677
11. Sano N, Ukita S (2006) Mater Chem Phys 99:447–450
12. Sevilla M, Lota G, Fuertes AB (2007) J Power Sources 171:546–551
13. Lee K, Zhang J, Wang H, Wilkinson DP (2006) J Appl Electrochem 36:507–522
14. Chai GS, Shin IS, Yu JS (2004) Adv Mater 16:2057–2061
15. Ren J, Ding J, Chan KY, Wang H (2007) Chem Mater 19:2786–2795
16. Chen SX, Zhang X, Shen PK (2006) Electrochem Commun 8:713–719
17. Yoon SB, Sohn K, Kim JY, Shin CH, Yu JS, Hyeon T (2002) Adv Mater 14:19–21
18. Fang B, Kim M, Yu JS (2008) Appl Catal B Environ 84:100–105
19. Kim JH, Fang B, Kim M, Yu JS (2009) Catal Today 146:25–30
20. Fiçicilar B, Bayrakçeken A, Eroğlu I (2009) J Power Sources 193:17–23
21. Fiçicilar B, Bayrakçeken A, Eroğlu I (2010) Int J Hydrogen Energy 35:9924–9933
22. Liu X, Tian B, Yu C, Gao F, Xie S, Tu B, Che R, Peng LM, Zhao D (2002) Angew Chem 41:3876–3878
23. Zhao D, Feng J, Huo Q, Melosh N, Fredrickson GH, Chmelka BF, Stucky GD (1998) Science 279:548–552
24. Buchel G, Unger KK, Matsumoto A, Tsutsumi K (1998) Adv Mater 10:1036–1038
25. Joo SH, Choi SJ, Oh I, Kwak J, Liu Z, Terasaki O, Ryoo R (2001) Nature 412:169–172
26. Kruk M, Jaroniec M (2001) Chem Mater 13:3169–3183
27. Jaroniec M, Solovyov LA (2006) Langmuir 22:6757–6760
28. Acharya CK, Li W, Liu Z, Kwon G, Turner CH, Lane AM, Nikles D, Klein T, Weaver M (2009) J Power Sources 192:324–329
29. Yu P, Pemberton M, Plasse P (2005) J Power Sources 144:11–20
30. Wang J, Yin G, Shao Y, Zhang S, Wang Z, Gao Y (2007) J Power Sources 171:331–339
31. Colon-Mercado HR, Popov BN (2006) J Power Sources 155:253–263
32. US DoE (2007) DOE cell component accelerated stress test protocols for PEM fuel cells. US DoE, USA. http://www1.eere.energy.gov/hydrogenandfuelcells/fuelcells/pdfs/component_durability_profile.pdf. Accessed 15 Jul 2011
33. Choo HS, Kinumoto T, Nose M, Miyazaki K, Abe T, Ogumi Z (2008) J Power Sources 185:740–746
34. Joo JB, Kim P, Kim W, Yi J (2006) J Electroceram 17:713–718
35. Ambrosio EP, Francia C, Manzoli M, Penazzi N, Spinelli P (2008) Int J Hydrogen Energy 33:3142–3314

36. Liu Z, Gan LM, Hong L, Chen W, Lee JY (2005) J Power Sources 139:73–78
37. Kim KS, Winograd N, Davis RE (1971) J Am Chem Soc 93:6296–6297
38. Dihkgraaf PJM, Duisters HAM, Kuster BJM, van der Wiele K (1988) J Catal 112:337–344
39. Kim HJ, Kim WI, Park TJ, Park HS, Suh DJ (2008) Carbon 46:1393–1400
40. Tamizhmani G, Dodelet JP, Guay D (1996) J Electrochem Soc 143:18–23
41. Zhao ZW, Guo ZP, Ding J, Wexler D, Ma ZF, Zhang DY, Liu HK (2006) Electrochem Commun 8:245–250
42. Stonehart O (1992) J Appl Electrochem 22:995–1001
43. Joo SH, Pak C, You DJ, Lee SA, Lee HI, Kim JM, Chang H, Seung D (2006) Electrochim Acta 52:1618–1626
44. Lei ZB, Bai SY, Xiao Y, Dang LQ, An LZ, Zhang GN, Xu Q (2008) J Phys Chem C 112:722–731
45. Liu ZL, Lee JY, Chen WX, Han M, Gan LM (2004) Langmuir 20:181–187
46. Liu SH, Yu WY, Chen CH, Lo AY, Wang BJ, Chen SH, Liu SB (2008) Chem Mater 20:1622–1628
47. Wen Z, Wang Q, Zhang Q, Li J (2007) Electrochem Commun 9:1867–1872
48. Kim S, Park S-J (2007) J Solid State Electrochem 11:821–828
49. Chai GS, Yoon SB, Yu J-S, Choi J-H, Sung Y-E (2004) J Phys Chem B 108:7074–7079
50. Dong L, Sanganna Gari RR, Li Z, Craig MM, Hou S (2010) Carbon 48:781–787
51. Wang Y, He C, Brouzgou A, Liang Y, Fu R, Wu D, Tsiakaras P, Song S (2012) J Power Sources 200:8–13
52. Hsieh C-T, Lin J-Y, Yang S-Y (2009) Physica E 41:373–378
53. Golikand AN, Maragheh MG, Sherehjini SS, Taghi-Ganji KM, Yari M (2006) Electroanalysis 18:911–917
54. Kim DB, Lim D-H, Chun H-J, Kwon H-H, Lee H-I (2010) Carbon 48:673–679
55. Iwasita T (2002) Electrochim Acta 47:3663–3674
56. Wu G, Li L, Xu BQ (2004) Electrochim Acta 50:1–10
57. Salvador-Pascual JJ, Collins-Martinez V, Lopez-Ortiz A, Solorza-Feria O (2010) J Power Sources 195:3374–3379
58. Elezovic NR, Babic BM, Radmilovic VR, Vracar LM, Krstajic NV (2009) Electrochim Acta 54:2404–2409
59. Joo SH, Kwon K, You DJ, Pak C, Chang H, Kim JM (2009) Electrochim Acta 54:5746–5753
60. Specchia S, Francia C, Spinelli P (2011) Polymer electrolyte membrane fuel cell. In: Liu RS, Zhang L, Sun X, Liu H, Zhang J (eds) Electrochemical technologies for energy storage and conversion, vol 2. Wiley-VHC, Weinheim, pp 601–670
61. Casalegno A, Marchesi R (2008) J Power Sources 175:372–382
62. Watanabe M, Tsurumi K, Mizukami T, Nakamura T, Stonehart P (1994) J Electrochem Soc 141:2659–2668
63. Ferreira PJ, la O' GJ, Shao-Horn Y, Morgan D, Makharia R, Kocha S, Gasteiger HA (2005) J Electrochem Soc 152:A2256–A2271
64. Ferreira PJ, Shao-Horn Y (2007) Electrochem Solid-State Lett 10: B60–B63
65. Gavello G, Zeng J, Francia C, Icardi UA, Graizzaro A, Specchia S (2011) Int J Hydrogen Energy 36:8070–8081